Talanta 82 (2010) 1455–1461

Contents lists available at ScienceDirect

Talanta

journal homepage: www.elsevier.com/locate/talanta

Hot electron induced cathodic electrochemiluminescence at AuSb alloy electrode for fabricating immunosensor with self-assembled monolayers

Ai-Hong Wu, Jian-Jun Sun*, Yi-Min Fang, Xiu-Li Su, Guo-Nan Chen

Key Laboratory of Analysis and Detection for Food Safety (Ministry of Education), and Fujian Provincial Key Laboratory of Analysis and Detection for Food Safety, Department of Chemistry, Fuzhou University, Fuzhou 350108, China

ARTICLE INFO

Article history:
Received 30 March 2010
Received in revised form 6 July 2010
Accepted 9 July 2010
Available online 16 July 2010

Keywords:
Cathodic electrochemiluminescence (ECL)
AuSb alloy electrode
Oxide film
Immunosensor
Human IgG

ABSTRACT

Thin antimony oxide covered AuSb alloy electrode was firstly found to be an excellent cold cathode for generating hot electrons during cathodic pulse polarization. Owing to the injection of hot electrons and the subsequent generation of hydrated electrons, fluorescein iso-thiocyanate (FITC) that cannot be excited in common ECL was cathodically excited at the alloy electrode. Self-assembled thiol monolayers were formed on the electrode surface due to the presence of Au in the alloy, to which strepavidin was covalently bound, and then biotinylated antibody was immobilized through the strepavidin–biotin interaction. As a simple model, an immunosensor for the detection of human IgG (hIgG) using FITC as labeling agent was fabricated. ECL signals were responsive to the amount of hIgG bounded to the immunosensor. The ECL intensity was linearly changed with the logarithm of hIgG concentration in the range of 1.0–1000 ng mL^{-1}, and the detection limit was ca. 0.3 ng mL^{-1} (S/N = 3). The proposed immunosensor showed a broad linear range (three magnitudes), good reproducibility and stability, which is promising in detecting FITC-based labels in various types of bioaffinity assays.

1. Introduction

Electrochemiluminescence (ECL) as an analytical tool is gradually gaining importance, especially in connection with the samples of biological origin, due to its sensitivity, selectivity, and simplified optical setup [1]. As an important branch of ECL, cathodic ECL has also become attractive owning to its unique advantages, such as a wide available potential window, high sensitivity in a wide linear range and a low detection limit [2]. Attributed to the injection of hot electrons into the aqueous solution and the subsequent generation of hydrated electrons as reducing mediators, various types of compounds including aromatic hydrocarbon [3], lanthanide and transition metal chelates [4], organic luminophores [5,6] and some biomolecules [7,8] are sensitively determined. Besides, fluorometric reagent such as fluorescein [9] and rhodamine B [10] that cannot be excited in common ECL was cathodic excited, which widened the application field of this method.

It has been previously suggested that oxide covered aluminium, magnesium [11], silicon [12] and glassy carbon [13] electrodes can act as cold cathodes during cathodic pulse polarization. However, because of the electrons trapped in oxide film layer, intrinsic ECL is produced at these electrodes, which is considered to be significant interference in the applications. Additionally, alkalization of Al_2O_3 and SiO_2 that destroyed the oxide film [14] is also a great limitation in the applications.

Self-assembled monolayers (SAMs) of thiol on Au have been widely studied [15,16]. The single molecular organized structures have numerous advantages [17], such as free of defects, nanostructures, much more stable, etc. Gold has been shown to be a good substrate for the immobilization of DNA and proteins via self-assembled thiol-COOH or thiol-NH_2 monolayers, owing to the strong bonds between sulfurs and Au [18–21].

AuSb alloy is a good semiconductor, in which a crystalline compound of Au with the polyvalent Sb is chemically formed [22]. It maintains the excellent corrosion resistance of Au, while the hardness is increased and melting temperature is lowered. Attributed to these special characteristics, AuSb alloy is widely used in semiconductor integrated circuits to reduce the ohmic resistance and thus reduce the dark current. In this work, the partially oxide covered AuSb alloy was firstly found to be an excellent electrode material for cathodic ECL, at which flourescein iso-thiocyanate (FITC) was cathodically excited. Self-assembled thiol monolayers can be formed on the alloy surface due to the presence of Au, which makes AuSb an attractive candidate in fabricating biosensors. As a simple model, an immunosensor based on cathodic ECL at the alloy electrode immobilized with an antibody by a self-assembled monolayer (SAM) of thiolacetic acid is fabricated. FITC-labeled hIgG is determined in a wide linear range

* Corresponding author. Tel.: +86 591 22866136; fax: +86 591 22866136.
E-mail address: JJSun@fzu.edu.cn (J.-J. Sun).

0039-9140/$ – see front matter © 2010 Elsevier B.V. All rights reserved.
doi:10.1016/j.talanta.2010.07.017

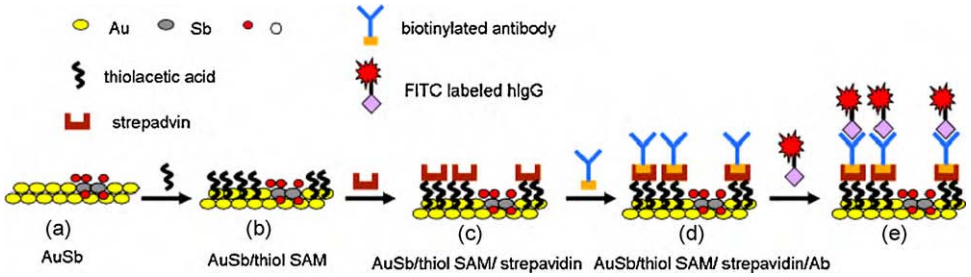

Scheme 1. Fabricating steps of the ECL immunosensor.

from 1.0 to 1000 ng ml^{-1}, and the detection limit is ca. 0.3 ng ml^{-1} (S/N = 3).

2. Experimental

2.1. Chemicals and materials

Human IgG (hIgG), biotinylated goat anti-human IgG, FTIC-labeled hIgG and FTIC-labeled goat IgG were purchased from Beijing Biosynthesis Biotechnology Co., Ltd. (Beijing, China). Thiolacetic acid, streptavidin (15.7 U mg^{-1}) and bovine serum albumin (BSA, 96–99%) were obtained from Sigma (St. Louis, MO). Boric acid borate buffer (BBS), 0.2 M, with various pH values were prepared by adjusting the pH with 0.1 M NaOH and H_2SO_4. Doubly distilled water was used throughout the experiments. Au (Φ 3 mm, Lanli Technology Co. Ltd., Tianjin, China) and AuSb (area ca. 44 mm^2) (AuSb, ChenDao Industrial. Co. Ltd., QingDao, China) were used as the working electrodes. The counter electrode was a platinum foil (area ca. 200 mm^2), while an Ag/AgCl (saturated KCl) electrode was used as a reference. Electrochemical impedance spectroscopy (EIS) is performed in 50 mM PBS (5 mM $Fe(CN)_6^{4-/3-}$ + 0.1 M KCl, pH 7.4).

2.2. Apparatus

Electrochemical measurements were performed at an electrochemical working station VMP3 (Princeton Applied Research Co., Ltd., USA). The pulse amplitude (E_f) varied from 0 to −16.0 V (vs. Ag/AgCl), and generally was set at −12.0 V if not specially mentioned. The pulse width was 0.4 ms, and the duration time was 9.6 ms. The time for applying pulse polarization equaled to the time for collecting ECL signals was 20 s. ECL signals were recorded by an Ultra-weak Chemiluminescence Analyzer (BPCL-K, Institute of Biophysics, Academia Silica, Beijing, China) controlled by a personal computer with 0.1 s sample interval. While collecting ECL signals, the cell was placed directly in front of the photomultiplier (PMT operated at −1000 V) and the PMT window was opened towards the working electrode only. X-ray photoelectron spectroscopy (XPS) was carried out at PHI Quantum scanning ESCA microprobe with Al $K\alpha_{1,2}$ radiation (1486.60 eV). All the spectra were obtained with a spot of 200 μm at a vacuum less than 5.0×10^{-8} mbar. X-ray fluorescence (XRF) was carried out at X-ray Fluorescence Spectrophotometer (PW 2424, Philips, Holland) and fluorescence spectra were measured in Cary Eclipse Fluorescence Spectrophotometer (Varian, Inc., USA). ECL spectra were measured using a series of filters with the wavelength of 400, 425, 495, 535, 555, 575, 595, 620, 640, 680 nm.

2.3. Pretreatment of the AuSb electrode

The AuSb electrode was firstly cleaned in boiled Piranha (30% H_2O_2:H_2SO_4 (V:V = 3:7)) for 5 min, and then mechanically polished with 0.3 μm Al_2O_3 and ultrasonicated in water for 3 min. Subsequently the electrode was immersed in the mixed solution of HNO_3:H_2O (V:V = 1:1) for 30 min and ultrasonicated in water for 3 min, and then dry in air for more than 24 h. Before use, the electrode was electrochemically cleaned by a linearly scanning potential between −0.2 and +1.6 V in 0.10 M H_2SO_4 and finally rinsed with water.

2.4. Construction of the immunosensor

A schematic diagram showing the steps of fabricating ECL immunosensor is given in Scheme 1. The cleaned oxide covered AuSb electrode was immersed in 200 μL of 10 mM thiolacetic acid in dark for 2 h at room temperature and then thoroughly rinsed with water (AuSb/thiol SAM). To obtain a layer of strepavidin, the electrode was immersed in a mixed solution of 1 mg mL^{-1} strepavidin, 10 mg mL^{-1} EDC and 20 mg mL^{-1} NHS at 37 °C for 30 min, thoroughly washed with water and then dried with a nitrogen stream. The AuSb/thiol SAM/strepavidin specimen was then immersed in 0.5 mg mL^{-1} biotinylated antibody solution (50 mM PBS, pH 7.4) at 37 °C for 30 min (AuSb/thiol SAM/strepavidin/Ab). Unreacted antibodies were then removed from the substrate by rinsing with 50 mM PBS, and then dried with nitrogen. Then the electrode was immersed in 2% BSA for 1 h to block nonspecific binding sites. After being rinsed with pH 7.4 PBS, the electrode was incubated in different concentrations of FITC-labeled hIgG samples at 37 °C for 1 h.

3. Results and discussion

3.1. Characterization of the oxidized AuSb alloy electrode

In order to get a general idea about the component of the bulk alloy and the surface oxide film, XRF and XPS were employed. XRF results show that the contents for Au and Sb in the bulk AuSb alloy are 99.19 and 0.61%, respectively. The atomic ratio of these two atoms is estimated to be ca. 100:1 (denoted as $Au_{100}Sb_1$).

Further understanding on the property of the oxide film can be obtained from XPS spectrum as shown in Fig. 1. Au, C, O and Sb are present on the original surface (Fig. 1A, curve a) with fractions of 41.8% (Au4f, 87.7 eV), 39.3% (C1s, 284.5 eV), 18.2% (Sb3d and O1s, 532.5 eV) and 0.7% (Sb4d, 35.2 eV), respectively. Because the binding energy value for O1s is very close to that for Sb3d [23], it is difficult to tell the individual contributions of them from the XPS survey. A high resolution Sb3d and O1s spectrum is also shown in Fig. 1B (curve a). Three peaks for O1s (529.2 eV), $Sb3d_{5/2}$ (532.0 eV) and $Sb3d_{3/2}$ (533.6 eV) are observed, and the atomic ratio of Sb3d and O1s is estimated to be ca. 7:2. If the component of Au is taken into consideration, the partially oxide covered AuSb electrode can be denoted as $Au_{41.8}Sb_{14.2}O_{4.1}$ (or $Au_{100}Sb_{34}O_{10}$), which is different from that of the bulk alloy ($Au_{100}Sb_1$). On this basis, it is concluded that the component of Sb is higher in the surface than in the bulk alloy, and a thin antimony oxide film is partially formed on the surface. However, it is difficult to separate the contributions of Sb^{3+} and Sb^{5+} in the oxide film probably due to the instrumental limitation of our spectrometer. According to ref. [24], Sb can be chemically

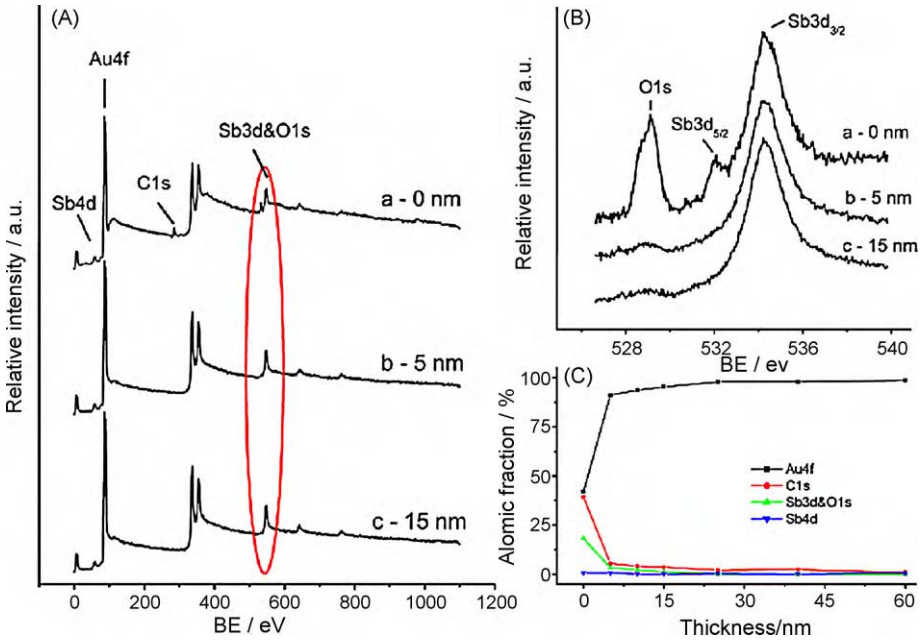

Fig. 1. (A) XPS survey and (B) Sb3d and O1s high resolution XPS spectra of the AuSb alloy electrode surface at different etching thicknesses. (C) Dependence of fractions of Au, C, O and Sb on the etching thickness.

oxidized by HNO_3 to form a resultant of $H[Sb(OH)_6]$ ($Sb_2O_5{\cdot}H_2O$). Therefore, it is assumed that Sb_2O_5 is the main form of the oxide in the AuSb alloy surface.

In order to define the thickness of the oxide film, the electrode surface was further etched by Ar^+ ion. XPS survey at the depth of 5 nm (curve b) and 15 nm (curve c) are also shown in Fig. 1A. Compared with that at the original surface (Fig. 1A, curve a), the peak for C1s disappears at the depth of 5 nm (Fig. 1A, curve b), suggesting that the large fraction of C1s (39.3%) on the original surface is mainly due to the adsorption of carbon dioxide in the air. Seem from the high resolution XPS spectra for Sb3d and O1s (Fig. 1B), significant decreases of the peaks for O1s and $Sb3d_{5/2}$ are observed at the depth of 5 nm (curve b) when compared with that at the original surface. And almost no differences between the case for 5 and 15 nm are found. Atomic fraction profile with depth can be obtained as shown in Fig. 1C.

As expected, the fraction of C1s steeply decreases to ca. 4.0% at the depth of 5 nm, and further to 0.9% at 15 nm. The fraction of Sb3d and O1s decreases steeply at the depth of 5 nm, indicting that the thickness of the oxide film is no more than 5 nm. Besides, the fraction for Sb4d keeps almost constant at ca. 0.7% during the whole etching process, almost the same as the final fraction of Sb3d (ca. 1.0%). On the contrary, the fraction of Au increases significantly from 41.8 to 98.5% at the depth of more than 15 nm. The atomic ratio of Au to Sb at the depth of ca. 15 nm is estimated to be ca. 99:1, agrees well with that form XRF (100:1), demonstrating a component similar to the bulk alloy is obtained.

The surface of the oxidized AuSb alloy electrode was further examined electrochemically in 0.1 M H_2SO_4 (Fig. 2). A control experiment was also carried out at an Au electrode. The oxidation peak of the adsorbed OH for the formation of Au $(OH)_x$ or AuO is at ca. 1.3 V, and the corresponding reduction peak at ca. 0.8 V [25] at both Au and the alloy electrode, indicating that the electrochemical behavior of AuSb alloy is similar to that of Au. However, the current density at AuSb alloy is smaller than that at Au electrode, suggesting a smaller active surface of gold. The active surface calculated by peak area at ca. 0.8 V (Fig. 2, frame) for the alloy is ca. 90% of that for Au, resulted from the formation of a thin oxide film that partly blocks the electron-transfer process on the electrode surface. A schematic representation for the structure of bulk alloy and the surface oxide film is outlined in the insert of Fig. 2.

3.2. Cathodic ECL of lumimophores at partially oxide covered AuSb alloy electrode

Thin oxide film coated electrode can act as pulsed cold cathodes emitting hot electrons into electrolyte solution, which makes the ECL generation from luminophore possible [2]. Herein, luminophores such as $Ru(bpy)_3^{2+}$, luminol and FITC were selected to examine the cathodic ECL behavior at partially oxide covered AuSb electrode. As a comparison, a control experiment was carried out at an Au electrode with the same pretreatment with AuSb as shown in Section 2.3. The results show that strong ECL signals are produced at the partially oxidized covered alloy electrode (Fig. 3A, curve a, b and c), but not at Au electrode (Fig. 3A, curve a′, b′ and c′), suggesting that antimony oxide covered on AuSb surface plays an important role in the luminescent process. Attributed to the

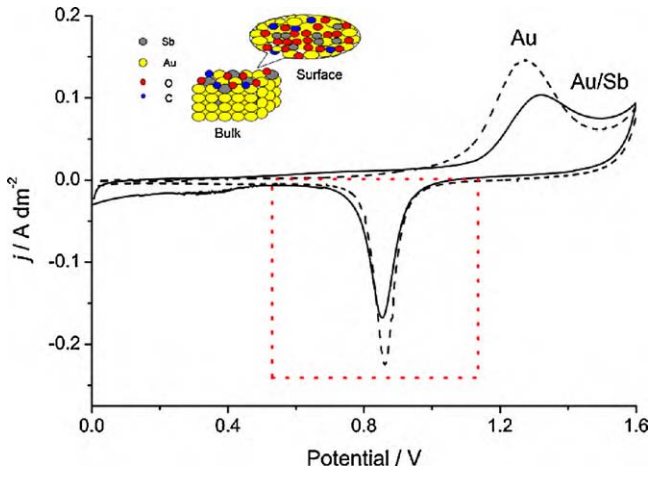

Fig. 2. Cyclic voltammetry plot of Au and AuSb electrodes in 0.1 M H_2SO_4. Scan rate: 0.1 V s^{-1}.

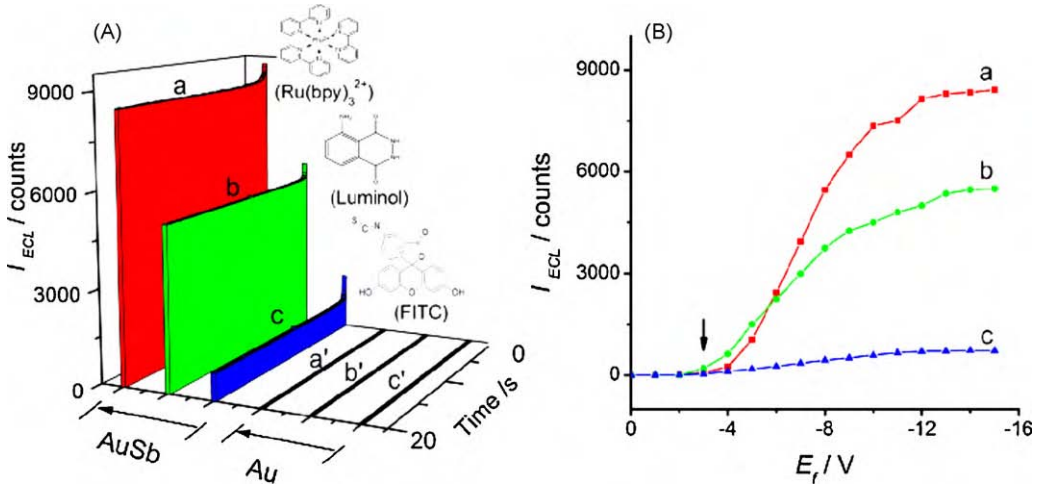

Fig. 3. (A) Cathodic ECL of luminophores at AuSb alloy and Au electrode at constant pulse amplitude of −12 V. (B) Effects of pulse amplitude (E_f) on the ECL intensity. Solution: 0.2 M borate buffer (pH 8.0) containing 0.1 M Na_2SO_4 and 1 mM $K_2S_2O_8$ with 1.0×10^{-5} M Ru(bpy)$_3^{2+}$ (a and a′), luminol (b and b′) or FITC (c and c′). Pulse width: 0.4 ms, duration time: 9.6 ms, total time: 20 s.

thin oxide film, energetic electrons can be produced through direct tunneling during cathodic pulse polarization. Such electrons would be converted to hydrated electrons (e_{aq}^-) after thermalization and salvation, and then induced the subsequent luminescence [26].

Effects of the applied pulse amplitude on ECL intensity were examined (Fig. 3B). The ECL onset potentials for Ru(bpy)$_3^{2+}$ (curve a), luminol (curve b) and FITC (curve c) are approximately −3.0 V (vs. Ag/AgCl), close to the conduction band edge of the water [26], demonstrating the electrochemical generation of energetic hydrated electrons (e_{aq}^-) by hot electrons injection into the conduction band of water [27,28] at the partially oxide covered AuSb alloy electrode.

3.3. Effects of e_{aq}^- scavengers on ECL intensity

Effects of e_{aq}^- scavengers on the cathodic ECL responses were examined in order to see whether e_{aq}^- were involved in the luminescent process. Fig. 4 displays the effects of fast e_{aq}^- scavenger (e.g. NO_2^-, NO_3^- and $Co(NH_3)_6^{3+}$) on the cathodic ECL at partially oxide covered AuSb alloy electrode. Take the case of FITC for an example, ECL intensity is reduced by the e_{aq}^- scavenger and heavily depends on the scavenger concentration. There is a great correspondence between the quenching capability ($NO_2^- < NO_3^- < Co(NH_3)_6^{3+}$) of these scavengers and the second-order reaction rate constants of them reacting with e_{aq}^- [29] [$k(e_{aq}^- + NO_2^-) = 4.1 \times 10^9 < k(e_{aq}^- + NO_3^-) = 9.7 \times 10^9 < k(e_{aq}^- + Co(NH_3)_6^{3+}) = 8.7 \times 10^{10}$]. The result further verifies the generation of e_{aq}^-, which is considered to be a key cathodic process to the ECL at thin insulating film covered electrode.

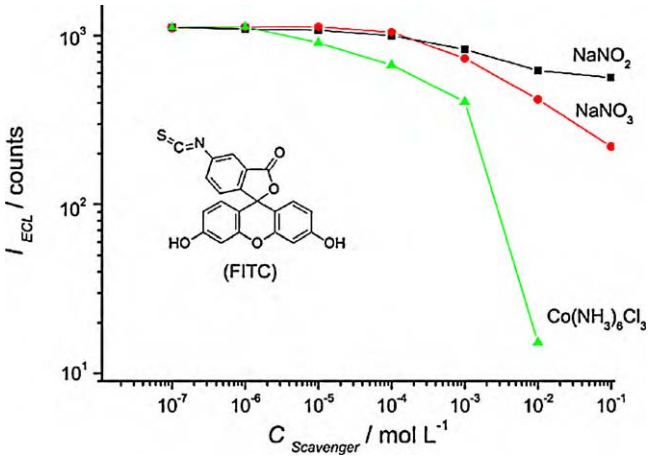

Fig. 4. Effect of e_{aq}^- scavengers NO_2^-, NO_3^- and $Co(NH_3)_6^{3+}$ on I_{ECL} of FITC at AuSb electrode. Solution: 0.2 M BBS (pH 8.0) containing 0.1 M Na_2SO_4, 1.0 mM $K_2S_2O_8$ and 1.0×10^{-5} M FITC. Pulse parameters as in Fig. 3A.

3.4. Possible ECL mechanism

The ECL spectra of the above three luminophores were collected as shown in Fig. 5. It should be mentioned that relative intensity of ECL and fluorescence are not in the same scale. The maximum emission wavelength in ECL spectrum is estimated by fitting the experimental data (dot) with Gaussian function. The ECL spectra (solid line) are identical to the fluorescence spectrum of them (dot-dash line), respectively, suggesting that emission is from the same excited singlet state.

Cathodic ECL of luminophores is induced by e_{aq}^- generated from the injection of energetic electrons into the electrolyte solution. The primary radicals for the observed cathodic ECL are similar to that described earlier [30,31]. Briefly, e_{aq}^- reacts with the coreactant ($S_2O_8^{2-}$) producing strong oxidizing species sulfate radicals ($SO^{\bullet}_4^-$) [29], which can further oxidize the luminophore to produce the luminescence. For example, in the case of FITC, fluorescein dianion (Flu^{2-}) is oxidized by $SO^{\bullet}_4^-$, and the resultant $Flu^{\bullet -}$ is reduced by e_{aq}^- to form the exciting state of Flu^{2-*}. After this, Flu^{2-*} would emit its fluorescence emission at ca. 520 nm. The possible mechanism is listed as follows:

$$e_{aq}^- + S_2O_8^{2-} \rightarrow SO_4^{2-} + SO^{\bullet}_4^- \quad (1)$$

$$Flu^{2-} + SO^{\bullet}_4^- \rightarrow Flu^{\bullet -} + SO_4^{2-} \quad (2)$$

$$Flu^{\bullet -} + e_{aq}^- \rightarrow Flu^{2-*} \quad (3)$$

$$Flu^{2-*} \rightarrow Flu^{2-} + h\nu \quad (520\,nm) \quad (4)$$

3.5. Fabrication and characterization of the immunosensor

Thin oxide film covered AuSb electrode is very attractive for fabricating cathodic ECL based biosensors. The reasons are as follows: (1) A chemically formed thin antimony oxide film covered on the alloy surface provides a premise for the cathodic excitation of luminophore. (2) A formation of self-assembled monolayer of thiol due to the special future of Au allows the immobilization

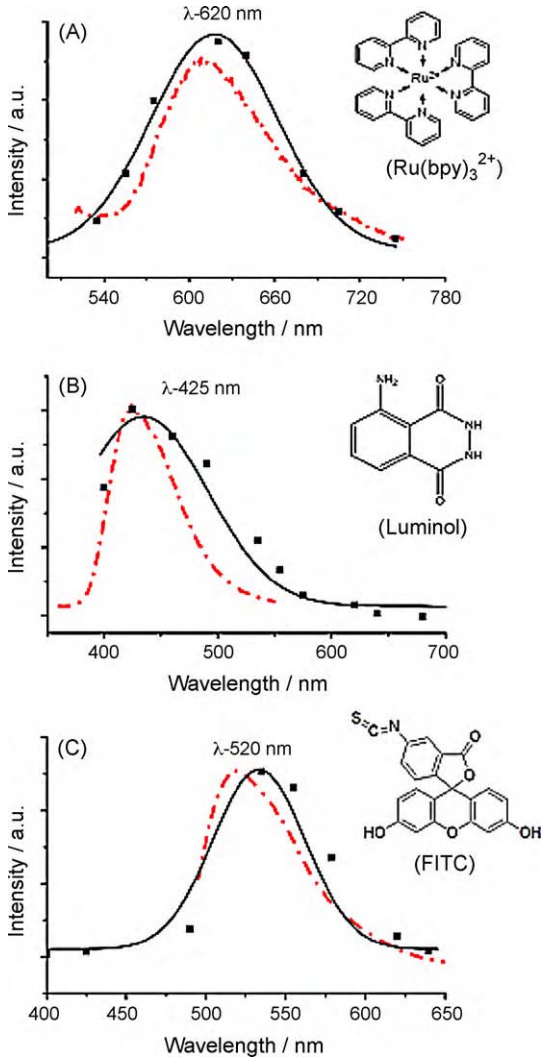

Fig. 5. Uncorrected ECL (square and solid line) and fluorescence emission (dash-dot line) spectra of (A) $Ru(bpy)_3^{2+}$, (B) luminol and (C) FITC. λ_{ex} for $Ru(bpy)_3^{2+}$, luminol and FITC are 455, 348 and 492 nm, respectively. Pulse amplitude: −12 V, other conditions are as in Fig. 3A. Relative intensity of ECL and fluorescence are not in the same scale.

of protein such as antibodies. In order to investigate whether a cathodic ECL based immunosensor can be fabricate on partially oxide covered AuSb electrode, a simple model with a direct determination method for determining FITC-labeled hIgG was proposed. Schematic representation for fabricating the ECL immunosensor (Scheme 1) shows that no ECL signal can be obtained at the specimens until the immunosesor was incubated with FITC-labeled hIgG. Herein, FITC-labeled hIgG was selected because it can be obtained commercially and cheaply, even though the ECL intensity was not so strong as luminol or $Ru(bpy)_3^{2+}$(see Fig. 3).

As an effective technique to monitor the surface feature and understand the chemical transformation [32], EIS is often employed to check the fabrication process of biosensors [33–35]. Nyquist plots of the electrode surface at different modification steps are shown in Fig. 6. The semicircle diameter at higher frequencies corresponds to the electron-transfer resistance (R_{ct}) and the linear part at lower frequencies corresponds to the diffusion process. The larger of the semicircle diameter, the larger the value of R_{ct} is.

The plot at the oxide covered AuSb electrode displays an almost straight line (Fig. 6, curve a), showing a characteristic of a mass diffusion limiting process. After a self-assemble thiol monolayer is on the electrode surface, an obvious resistant semicircle in the EIS

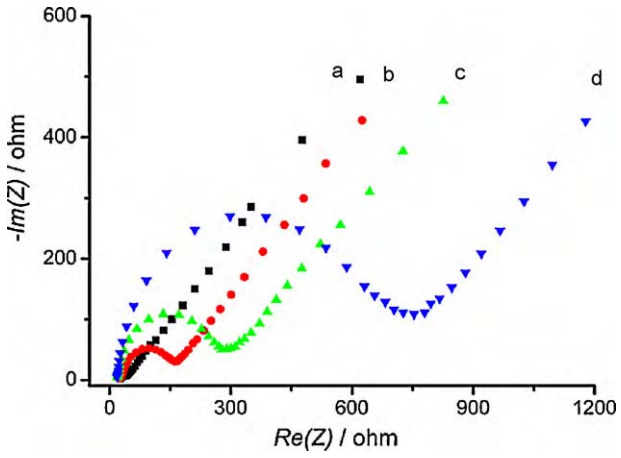

Fig. 6. Nyquist plots at (a) AuSb, (b) AuSb/thiol SAM, (c) AuSb/thiol SAM/strepavidin and (d) AuSb/thiol SAM/strepavidin/Ab in 50 mM PBS (5 mM $Fe(CN)_6^{4-/3-}$ + 0.1 M KCl, pH 7.4). The frequency range is between 0.01 and 200 kHz with signal amplitude of 10 mV.

occurred is formed with a value of R_{ct} = 160 Ω (Fig. 6, curve b). The further immobilization of strepavidin makes an increase in R_{ct} to ca. 300 Ω (Fig. 6, curve c). In the final step, the immobilization of biotinaylated antibody further increased the R_{ct} to ca. 750 Ω (Fig. 6, curve d) due to the avidin–biotin reaction, in which four molecules of biotinaylated antibodies can be bonded to one strepavidin.

3.6. Performance of the immunosensor

To assess the sensitivity and dynamic working range of the proposed immunoassay, the fabricated immunosensor was incubated with different concentrations of FITC-labeled hIgG. Herein, ECL intensity was responsive to the amount of hIgG bounded to the immunosensor (Fig. 7), which is related to the "bulk concentration" under the same condition when adsorption equilibrium is reached. The datasets of ECL intensity and FITC-labeled hIgG concentration were analysis by sigmoidal function, the results agree well with Langmuir adsorption isotherm equation. Besides, it was found that ECL intensity was linear increased with logarithmic of hIgG concentration. The standard calibration curve for hIgG detection is shown in the insert of Fig. 7, the ECL intensity (integrates of 20 s) is linearly changed with the logarithm of hIgG concentration in a wide concentration range from 1.0 to 1000 ng ml^{-1}, and the detection limit was ca. 0.3 ng ml^{-1} (S/N = 3).

The stability of the Au–S bond in the SAM was examined by continuously exacting the immunosensor after it was incubated with FITC-labeled hIgG. Relative standard deviation (RSD) of the ECL intensity for continuously excitation was 6.32% (n = 9), showing that the Au–S bond in the SAM was not reduced during such a negative pulse polarization. The lifetime of the immunosensor also can be evaluated from the RSD value above. The long-term stability of the fabricated immunosensor was also examined by comparing the ECL responses of the sensor to one hIgG level when stored in PBS (pH 7.4) at 4 °C for different time period. An excellent long-term stability was found within 4 weeks, which can be attributed to the strong bounds between Au and thiol SAMs.

The reproducibility of the immunosensor was estimated using five parallel sensors when determining one hIgG level (10.0 ng mL^{-1}). As shown in Fig. 8A, insignificant differences among the ECL signals are observed, indicating the immunosensor is quite reproducible and repeatable. RSD for the five fabricated sensors is found to be 5.03%.

Furthermore, the specificity of the immunosensor was investigated. The ECL response of the sensor to 10.0 ng mL^{-1} of

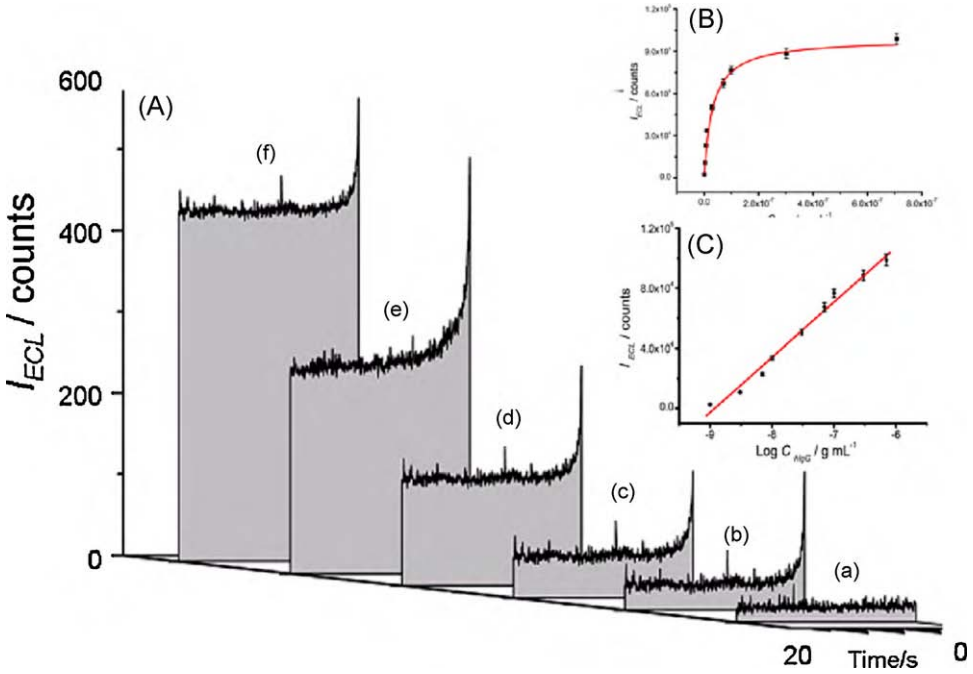

Fig. 7. (A) ECL responses of the immunosensor when incubated with (a) 1.0 ng mL^{-1}, (b) 3.0 ng mL^{-1}, (c) 7.0 ng mL^{-1}, (d) 30 ng mL^{-1}, (e) 100 ng mL^{-1} and (f) 700 ng mL^{-1} FITC-labeled hIgG. (B) Relationship between I_{ECL} and hIgG concentration when simulated by sigmoidal function. (C) Calibration curve for hIgG detection. ECL intensity are the integrate value of 20 s. The signals are average values of three parallel measurements. Solution: 0.2 M borate buffer (pH 8.0) containing 0.1 M Na_2SO_4 and 1 mM $K_2S_2O_8$. Pulse parameters as in Fig. 3A.

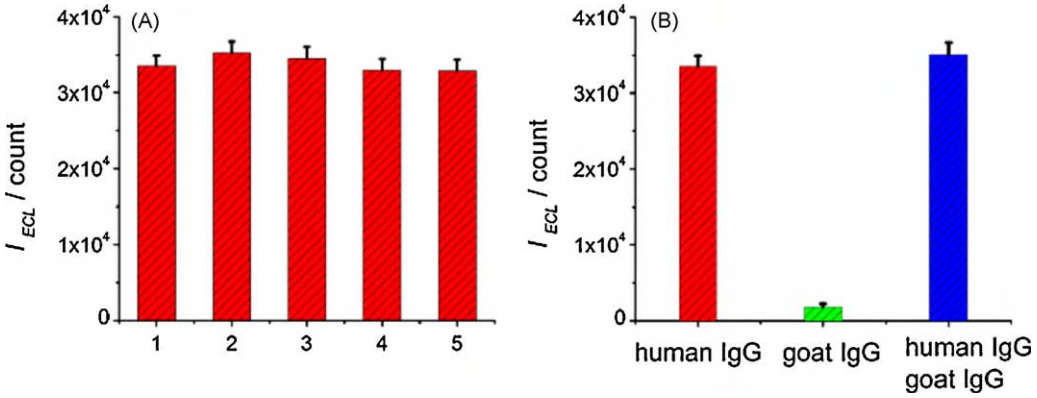

Fig. 8. (A) ECL signals obtained at five parallel sensors. (B) Sensor response to 10 ng mL^{-1} hIgG, goat IgG and the mixed solution of hIgG and goat IgG. ECL conditions are as in Fig. 7.

FITC-labeled hIgG, 10.0 ng mL^{-1} of FITC-labeled goat IgG and 10.0 ng mL^{-1} of the mixed solution of them were examined. As shown in Fig. 8B, the ECL response to nonspecific goat IgG is ca. 5.0% of that to hIgG. Furthermore, no significant differences (signal difference < 5%) were observed between the signals to hIgG and the mixed one of hIgG and goat hIgG, indicating that the goat IgG could not cause any obvious interference.

4. Conclusions

The present work was carried out to explore the possibility of the use of stable oxide covered AuSb as an electrode material, and the possibility to fabricate a cathodic ECL based immunosensor through SAMs using FITC as labeling agent. Thin oxide film was formed on the AuSb alloy electrode surface after being chemically oxidized, which was proved to be suitable for injecting hot electrons into the electrolyte solution during cathodic pulse polarization. Cathodic ECL of FITC was produced due to the hot electrons generated through the thin antimony oxide film. A cathodic ECL based immunosensor for the determination of hIgG was fabricated on partially oxide covered AuSb alloy electrode with SAMs. FITC-labeled hIgG was determined in a wide linear range from 1.0 to 1000 ng ml^{-1}, with a detection limit of ca. 0.3 ng ml^{-1} (S/N = 3). Actually, the detection limit can be much improved if an more efficient luminophore, such as $Ru(bpy)_3^{2+}$, is used.

Acknowledgements

The authors thank for the financial support from the National Science Foundation of China (Nos. 20775015, 20735002, and 20975022), National Basic Research Program of China (No. 2010CB732403), Specialized Research Fund for Doctoral Program of Higher Education (20070386005) from MOE, the program for NCETTFJ (XSRC2007-02).

References

[1] M.M. Richter, Chem. Rev. 104 (2004) 3033–3036.
[2] S. Kulmala, J. Suomi, Anal. Chim. Acta 500 (2003) 21–69, and references therein.
[3] K. Haapakka, J. Kankare, K. Lipiainen, Anal. Chim. Acta 215 (1988) 341–345.
[4] T. Ala-Kleme, M. Latva, H.K. Aapakka, Anal. Chim. Acta 403 (2000) 161–171.
[5] Y.E. Sung, A.J. Bard, J. Phys. Chem. B 102 (1998) 9806–9811.
[6] Q. Jiang, A.M. Spehar, M. Håkansson, J. Suomi, T. Ala-Kleme, S. Kulmala, Electrochim. Acta 51 (2006) 2706–2714.
[7] T. Ala-Kleme, P. Ma1kinen, T. Ylinen, L. Va1re, S. Kulmala, P. Ihalainen, J. Peltonen, Anal. Chem. 78 (2006) 82–88.
[8] A. Spehar-Deleze, J. Suomi, Q. Jiang, N. Rooij, M. Koudelka-Hep, S. Kulmala, Electrochim. Acta 51 (2006) 5438–5444.
[9] J. Suomi, T. Ylinen, M. Håkansson, M. Helin, Q. Jiang, T. Ala-Kleme, S. Kulmala, J. Electroanal. Chem. 586 (2006) 49–55.
[10] M. Hakansson, Q. Jiang, M. Helin, M. Putkonen, A.J. Niskanen, S. Pahlberg, T. Ala-Kleme, L. Heikkila, J. Suomi, S. Kulmala, Electrochim. Acta 51 (2005) 289–296.
[11] Q. Jiang, A. Spehar, M. Håkansson, J. Suomi, T. Ala-Kleme, S. Kulmala, Electrochim. Acta 51 (2006) 2706–2714.
[12] Q. Jiang, H. Ketamo, A.J. Niskanen, J. Suomi, M. Håkansson, S. Kulmala, Electrochim. Acta 51 (2006) 3332–3337.
[13] A.H. Wu, J.J. Sun, R.J. Zheng, H.H. Yang, G.N. Chen, Talanta 81 (2010) 934–940.
[14] S. Kulmala, Academic dissertation, Finland, Turku, 1995.
[15] D.B. Colin, E.B. Troughton, Y.T. Tao, J. Erall, M.W. George, G.N. Ralph, J. Am. Chem. Soc. 111 (1989) 321–325.
[16] M. Dijksma, B. Kamp, J.C. Hoogvliet, W.P. Bennekom, Langmuir 16 (2000) 3852–3857.
[17] M.M. Vladimir, TrAC, Trends Anal. Chem. 21 (2002) 439–450.
[18] X.H. Xu, A.J. Bard, J. Am. Chem. Soc. 117 (1995) 2627–2631.
[19] R. Levicky, T.M. Herne, M.J. Tarlov, S.K. Satija, J. Am. Chem. Soc. 120 (1998) 9787–9792.
[20] N. Patel, M.C. Davies, M. Hartshorne, R.J. Heaton, C.J. Roberts, S.J.B. Tendler, P.M. Williams, Langmuir 13 (1997) 6485–6490.
[21] X. Sun, P. He, S. Liu, J. Ye, Y. Fang, Talanta 47 (1998) 487–495.
[22] H.G. Boyen, A. Cossy-Favre, P. Oelhafen, A. Siber, P. Ziemann, C. Lauinger, T. Moser, P. Häussler, F. Baumann, Phys. Rev. B 51 (1995) 1791–1802.
[23] F. Garbassi, Surf. Interface Anal. 2 (1980) 165–169.
[24] W.A. Badawy, Thin Solid Films 186 (1990) 59–72.
[25] S.Y. Quek, C.M. Friend, E. Kaxiras, Surf. Sci. 600 (2006) 3388–3393.
[26] S. Kulmala, T. Ala-Kleme, A. Hakanen, K. Haapakka, J. Chem. Soc., Faraday Trans. 93 (1997) 165–168.
[27] Y.E. Sung, F. Gaillard, A.J. Bard, J. Phys. Chem. B 102 (1998) 9797–9805.
[28] F. Gaillard, Y.E. Sung, A.J. Bard, J. Phys. Chem. B 103 (1999) 667–672.
[29] G. Buxton, C. Greenstock, W. Helman, A. Ross, J. Phys. Chem. Ref. Data 17 (1988) 513–886.
[30] S. Kumala, T. Ala-Kleme, L. Heikkila, L. Vare, J. Chem. Soc., Faraday Trans. 93 (1997) 3107–3113.
[31] S. Kumala, T. Ala-Kleme, H. Joela, A. Kumala, J. Radioanal. Nucl. Chem. 232 (1998) 91–95.
[32] A.J. Bard, L.R. Faulkner, Electrochemical Methods: Fundamentals and Applications, 2nd ed., Wiley, New York, 1980.
[33] G. Jie, J. Zhang, D. Wang, C. Cheng, H. Chen, J. Zhu, Anal. Chem. 80 (2008) 4033–4039.
[34] Y. Li, H. Qi, Y. Peng, J. Yang, C. Zhang, Electrochem. Commun. 9 (2007) 2571–2575.
[35] W. Yao, L. Wang, H. Wang, X. Zhang, L. Lu, Biosens. Bioelectron. 24 (2009) 3269–3274.